Yanting Sun[1]
Boli Hu[2]
Chengfei Fan[1]
Lu Jia[1]
Yina Zhang[1]
Aifang Du[1]
Xiaojuan Zheng[1,3]*
Jiyong Zhou[1,2,3]

[1]Key Laboratory of Animal Virology of Ministry of Agriculture, Zhejiang University, Hangzhou, P. R. China
[2]College of Veterinary Medicine, Nanjing Agricultural University, Nanjing, P. R. China
[3]State Key Laboratory and Collaborative Innovation Center for Diagnosis and Treatment of Infectious Diseases, The First Affiliated Hospital, Zhejiang University, Hangzhou, P. R. China

Received January 9, 2015
Revised March 22, 2015
Accepted March 25, 2015

Research Article

iTRAQ-based quantitative subcellular proteomic analysis of *Avibirnavirus*-infected cells

Infectious bursal disease virus (IBDV) enters the host cells via endocytic pathway to achieve viral replication in the cytoplasm. Here, we performed LC-MS/MS coupled with isobaric tags for relative and absolute quantification labeling of differentially abundant proteins of IBDV-infected cells using a subcellular fractionation strategy. We show that the viral infection regulates the abundance and/or subcellular localization of 3211 proteins during early infection. In total, 23 cellular proteins in the cytoplasmic proteome and 34 in the nuclear proteome were significantly altered after virus infection. These differentially abundant proteins are involved in such biological processes as immune response, signal transduction, RNA processing, macromolecular biosynthesis, energy metabolism, virus binding, and cellular apoptosis. Moreover, transcriptional profiles of the 25 genes corresponding to the identified proteins were analyzed by quantitative real-time RT-PCR. Ingenuity Pathway Analysis clustered the differentially abundant proteins primarily into the mTOR pathway, PI3K/Akt pathway, and interferon-β signaling cascades. Confocal microscopy showed colocalization of the viral protein VP3 with host proteins heterogeneous nuclear ribonucleoprotein H1, nuclear factor 45, apoptosis inhibitor 5, nuclear protein localization protein 4 and DEAD-box RNA helicase 42 during the virus infection. Together, these identified subcellular constituents provide important information for understanding host–IBDV interactions and underlying mechanisms of IBDV infection and pathogenesis.

Keywords:
IBDV-infected cells / iTRAQ / Subcellular proteomics

DOI 10.1002/elps.201500014

Additional supporting information may be found in the online version of this article at the publisher's web-site

1 Introduction

Avibirnavirus infectious bursal disease virus (IBDV), belonging to the Birnaviridae family, is a pathogenic agent of a highly contagious disease that damages immature B lymphocytes in the bursa of Fabricius in poultry and causes severe immunodeficiency and mortality [1]. IBDV has a bisegmented double-stranded RNA genome (segments A and B) [2]. The large ORF of the segment A encodes a polyprotein that can undergo cotranslational self-proteolytic processing and release three polypeptides, the precursor capsid protein (pVP2), the protease VP4 and the multifunctional polypeptide VP3. The small ORF in segment A encodes a nonstructural protein VP5 with a molecular weight of 17 kDa. Segment B contains

Correspondence: Dr. Jiyong Zhou, Key Laboratory of Animal Virology of Ministry of Agriculture, Zhejiang University, 866 Yuhangtang Road, Hangzhou 310058, P. R. China
E-mail: jyzhou@zju.edu.cn
Fax: +86-571-8898-2218

Abbreviations: API5, apoptosis inhibitor 5; **CEF**, chicken embryo fibroblast; **DDX1**, DEAD-box RNA helicase 1; **DDX42**, DEAD-box RNA helicase 42; **FASP**, filter aided sample preparation; **GO**, Gene Ontology; **hnRNPH1**, heterogeneous nuclear ribonucleoprotein H1; **IBDV**, infectious bursal disease virus; **IBV**, infectious bronchitis virus; **IFA**, indirect immunoinfluscent assay; **IFIT5**, tetratricopeptide repeat 5; **iTRAQ**, isobaric tags for relative and absolute quantification; **JEV**, Japanese encephalitis virus; **mTOR**, mechanistic target of rapamycin(serine/threonine); **NF45**, nuclear factor 45; **pAb**, polyclonal antibody; **PRDX4**, peroxiredoxin 4; **PI3K/Akt**, phosphatidy linositol 3 kinase/protein kinase B; **STAT1**, signal transducer and activator of transcription 1

*Additional corresponding author: Dr. Xiaojuan Zheng
E-mail: zhengxiaojuan@zju.edu.cn

Colour Online: See the article online to view Figs. 1–3 and 6–8 in colour.

a single ORF encoding the RdRp VP1 polypeptide. In 2007, a cDNA microarray was used to analyze the differentially abundant transcripts of IBDV-infected chicken embryo fibroblasts (CEFs), which provides an overview of the mRNA profiles of cells during virus infection [3]. However, mRNA is not always the same with the protein level. Consequently, potential cellular factors involved in viral infection are more likely obtained from the proteomic profile of the host cellular response.

Now, large-scale screening is well recognized to be very effective for identifying host proteins of interest, many of which are unexpected and may lead to new discoveries regarding the host–virus interactions after additional functional validation. In the past decade, researchers have been paying increasingly close attention to the host response to virus infection at the translational level. 2DE coupled with MALDI-TOF MS has been widely applied to detecting the dynamics of host–pathogen interactions at various stages of virus infection [4–12]. However, proteins with low abundance and those that are very large or very small have been proven to be difficult to resolve using 2DE gels [13].

Using isobaric tags for relative and absolute quantification (iTRAQ) combined with LC and ESI-MS/MS analysis is emerging as a powerful methodology in the search for disease-specific targets [14]. In the past few years, iTRAQ has been used to explore and discover previously unidentified factors in the cell proteomic response to infection with porcine circovirus type 2 [15], porcine reproductive and respiratory syndrome virus [16], human immunodeficiency virus 1 [17], human papilloma virus [18], simian immunodeficiency virus [19] and influenza virus [20]. However, iTRAQ was rarely used to determine the subcellular proteomic response to IBDV infection. In this study, we utilized an iTRAQ-based quantitative subcellular proteomics approach followed by bioinformatic analysis and Western blot coupled with quantitative real-time RT-PCR and colocalization assays to observe the differentially abundant proteins profiles of IBDV-infected cells at 24 h after inoculation. We find that viral infection regulates the abundance and/or subcellular localization of more than 1000 host proteins in either the nuclear or the cytoplasmic fraction at the early phase of infection. These data provide clues to further understanding the replication and pathogenesis of IBDV and virus–host interactions.

2 Materials and methods

2.1 Cell culture, virus infection, and sample preparation

IBDV NB strain with CPE characteristics, including the infected cells became round, increasing light refrangibility, netting, and nucleus broken, was propagated in CEF as previously described [21, 22]. DF-1 cells (ATCC CRL-12203) were continuous cell line of CEF and routinely cultured at 39°C with 5% CO_2 in DMEM (Invitrogen, Carlsbad, CA) supplemented with 10% fetal bovine serum (GibcoBRL Life Technologies, Grand Island, NY). DF-1 cell monolayers were inoculated with the NB strain ($10^{7.2}$ $TCID_{50}$/0.1 mL) at a multiplicity of infection (MOI) of 1. Mock-infected DF-1 cells were used as the negative control. The IBDV- and mock-infected cells were harvested at 24 h postinfection (hpi) through scraping followed by centrifugation at 5000 × *g* for 10 min. Each sample of cells was washed thrice with ice-cold PBS followed by subcellular fractionation.

2.2 Flow cytometry analysis

IBDV- and mock-infected DF-1 cells were harvested at 24 hpi for the flow cytometric determination of IBDV infection [23]. Cells were washed twice with 1× PBS followed by fixation in 4% paraformaldehyde at room temperature for 30 min and subsequently permeabilized with 0.1% Triton X-100 in PBS for 10 min at room temperature. After washing twice with PBS, cells were incubated with the FITC-labeled anti-VP4 mAb at 4°C for 1 h in the dark. Cells were washed twice with 1× PBS, resuspended in 1 mL PBS, and analyzed by the flow cytometry (Beckman Coulter, Miami) using Flowjo7.6™ software. The percentage of IBDV–positive cells was calculated from the FITC fluorescence histogram using a region that was defined based on analysis of the noninfected control.

2.3 Subcellular fractionation

According to the manufacturer's instructions, cytosolic and nuclear protein fractions were sequentially extracted by the ProteoExtract® Subcellular Proteome Extraction Kit (Merck, Darmstadt, Germany). Briefly, cells were harvested by centrifugation at 600 × *g* for 10 min at 4°C and washed twice with cold wash buffer. Thereafter, the cells were resuspended in 1 mL of cytosol extraction buffer containing protease inhibitor cocktail (included in the fractionation kit), incubated for 10 min at 4°C with gentle agitation and centrifuged at 4°C at 800 × *g* for 10 min. The resultant supernatant was harvested and considered as the cytosolic fraction. The membranes and membrane organelles were dissolved with extraction buffer II. Subsequently, the pellets were resuspended in 500 μL nuclear extraction buffer containing a protease inhibitor mixture and Benzonase® Nuclease, incubated at 4°C for 10 min and centrifuged at 7000 × *g* for 10 min. The supernatant containing predominantly nuclear proteins was collected. Finally, protein concentrations were measured using a BCA Protein Assay Kit (Novagen, Darmstadt, Germany).

2.4 Protein digestion, peptide quantitative, and iTRAQ labeling

In the light of the previously FASP (filter aided sample preparation) procedure, proteins were digested [24]. First, 300 μg of protein for each sample was merged into 30 μL STD buffer (100 mM DTT, 4% SDS, 150 mM Tris-HCl pH 8.0). Next, UA buffer (8 M Urea, 150 mM Tris-HCl pH 8.0) removed the

DTT and detergent components by ultrafiltration (Microcon units, 30 kDa). Afterwards, the samples were incubated with 100 μL 0.05 M iodoacetamide in UA buffer for 20 min in the dark. At last, 40 μL trypsin buffer (2 μg trypsin in 40 μL dissolution buffer) was added to the protein suspensions digested overnight at 37°C. The peptides were measured by UV density at 280 nm.

Each sample about 32 μg was labeled using iTRAQ reagent 8-plex Multiplex Kit in accordance with the manufacturer's instructions (Applied Biosystems). The cytoplasmic fractions (F1) of IBDV-infected samples including three biological repeats were labeled as (Sample1)-113, (Sample2)-114 and (Sample3)-115, respectively, while mock-infected samples were labeled as (Sample4)-116, (Sample5)-117 and (Sample6)-118. The nuclear fraction (F2) samples were labeled similarly.

2.5 Peptide fractionation and LC-MS/MS analysis

Peptides labeled with iTRAQ were fractionated by strong cation exchange (SCX) chromatography using the AKTA Purifier system (GE Healthcare). After reconstituted and acidified with 2 mL buffer A (10 mM KH_2PO_4 in 25% of ACN, pH 2.7), the dried peptide mixture was loaded onto a PolySULFOETHYL 4.6 × 100 mm column (5 μm, 200 Å, PolyLC, MD, USA). Then, the peptides were eluted at flow velocity of 1 mL/min with a gradient of 0–10% buffer B (500 mM KCl, 10 mM KH_2PO_4 in 25% of ACN, pH 2.7) for 2 min, 10–20% buffer B for 25 min, 20–45% buffer B for 5 min, and 50–100% buffer B for 5 min. The fractions were collected every 1 min and the elution process was monitored by absorbance at 214 nm. The collected fractions were desalted on C18 Cartridges (Empore™ SPE Cartridges C18 [standard density], bed id 7 mm, volume 3 mL, Sigma) and then combined into six pools. Each fraction was concentrated by vacuum centrifugation following reconstituted in 40 μL of 0.1% (v/v) TFA. Afterwards, the samples were performed using Q Exactive mass spectrometer that was coupled with the Easy nLC apparatus (Thermo Fisher Scientific). The samples were added into C18-RP column (10 cm long, 75 μm inner diameter, 3 μm resin) in buffer A (0.1% formic acid in water), and then separated with buffer B (80% ACN in 0.1% formic acid) by IntelliFlow technology. The MS data were collected in accordance with following methods: after each full scan collected ten fragment patterns (MS2 scan).

2.6 Database search and quantification analysis

MS/MS data were searched and quantified using Maxquant (version: 1.3.0.5, Max Planck Institute of Biochemistry, Martinsried, Germany). The search identification was based on the Uniprot *Gallus gallus* (29 345 sequences, downloaded on March 25, 2013) and Uniprot IBDV (2692 sequences, downloaded on June 20, 2013) databases. The parameters of protein identification were as follows: peptide mass tolerance = 20 ppm, MS/MS tolerance = 0.1 Da, enzyme = trypsin, missed cleavage = 2; fixed modification: carbamidomethyl (C), iTRAQ8plex (K), iTRAQ8plex (N-term), variable modification: oxidation (M), FDR ≤ 0.01. The protein identification that was inferred from the unique peptide identification in three independent biological replicates was considered. In addition, a *p*-value less than 0.05 was considered to be statistically significant. The fold changes ≥1.2 or ≤0.83 of proteins were designated significant.

2.7 Quantitative real-time RT-PCR

We have designed specific primers (Supporting Information Table 1) to amplify target genes corresponding to the MS/MS-identified proteins. Using cDNA from IBDV-infected DF-1 cells, gene products were analyzed using the 7500 real-time PCR system (Applied Biosystems). The reaction contained 200 ng of cDNA template, 200 nM of each primer, and 1× SYBR premix Ex Taq (Perfect Real Time, TakaRa, Dalian, China), supplemented with water to a total volume of 20 μL. After an initial denaturation at 95°C for 30 s, the samples were amplified by 40 cycles of 95°C for 5 s and 60°C for 34 s. We obtained the melting curves, and then performed quantitative analysis of the data by the 7500 System SDS software version 1.3.1 (Applied Biosystems) with relative quantification (cycle threshold [Δ Δ Ct]) method. Simultaneously, mock-infected samples in parallel were used as negative controls.

2.8 Western blot analysis

In order to evaluate the differentially abundant proteins identified by iTRAQ-labeled LC-MS/MS system, IFN-induced protein with tetratricopeptide repeats 5 (IFIT5), signal transducer and activator of transcription 1 (STAT1), nuclear factor 45 (NF45), heterogeneous nuclear ribonucleoprotein H1 (hnRNPH1), and apoptosis inhibitor 5 (API5) were selected for Western blot analysis. Equal amounts of proteins from each sample were separated on 8% SDS-PAGE gels and transferred to NC membranes (Amersham Biosciences, Berks, UK) by using a semidry transfer cell (Bio-Rad Trans-blot SD). The membranes were blocked with 5% nonfat dried milk and then stained with a rabbit anti-STAT1 mAb (Epitomics, Cambridge, UK), mouse polyclonal antibody (pAb) to IFIT5 prepared in our laboratory (unpublished data), goat anti-NF45 pAb, goat anti-hnRNPH1 pAb, rabbit anti-API5 pAb, or rabbit anti-API5 pAb (Santa Cruz Biotechnology, Santa Cruz, CA). After washing three times with 0.05% Tween-20 in PBS (PBST), the membranes were incubated with horseradish peroxidase (HRP) conjugated goat anti-mouse IgG, HRP-conjugated goat anti-rabbit IgG, or HRP-conjugated donkey anti-goat IgG (Kirkegarard & Perry Laboratories, Gaithersburg, MD) at 37°C for 1 h. Finally, the detection was performed using chemiluminescence luminal reagents (SuperSignalWest Pico Trial Kit, Pierce, Rockford, IL).

2.9 Confocal immunofluorescence assay

DF-1 cells inoculated with IBDV at MOI = 1 were cultured for 24 h. At the end of this infection period, the cells were fixed with cold acetone/methanol (1/1) for 20 min at −20°C, and then dried in air. Fixed cells were incubated with a pAb adding to the NF45, hnRNPH1, API5, nuclear protein localization protein 4 (NPL4), and DDX42 at 37°C for 90 min. After washing three times with PBST, the cells were incubated with FITC-conjugated goat anti-rabbit IgG (Sigma), FITC-conjugated rabbit anti-goat IgG, and Alexa Fluor 566 goat anti-mouse IgG (Life Technologies) for 1 h at 37°C. Next, cell nuclei were stained blue using 4′,6-diamidino-2-phenylindole (DAPI, Sigma). Finally, the cells were washed three times with PBS and visualized using a Zeiss LSM780 laser confocal microscope.

2.10 Protein networks analysis

In order to gain further insight into the most relevant interaction networks and biological functions of the differentially abundant proteins, data of all proteins were analyzed using Ingenuity Pathway Analysis (IPA, Ingenuity Systems, www.ingenuity.com). Network construction was carried out as described previously [25]. In other words, we uploaded differentially abundant proteins (showing fold change of ≥1.2 or ≤0.83) identified into the IPA application, and then constructed the interaction network. Possible connections between those mapped genes were evaluated on the basis of knowledge curated in the IPA database. Each protein represented a node, and the interaction relationships between the nodes were linked by line. The linkages have been supported by at least one or more reference. Different shapes and the color of nodes represented differentially abundance and the functional classes of the proteins, respectively. Furthermore, IPA-curated canonical pathways were used to explore possible metabolic and cell signaling pathways.

3 Results

3.1 Quantitative subcellular proteome of IBDV-infected DF-1 cells

For analysis of the subcellular proteome, DF-1 cells were first infected with IBDV for 12, 18, 21, and 24 h. To select the optimal time point for iTRAQ analysis, virus infection profiles were identified by IFA using a mAb to VP3 protein of IBDV as the primary antibody. IFA results revealed that IBDV-specific immunofluorescence was observed at 12, 18, 21, and 24 hpi (with the monolayer appearing nearly 90% positive at the last time point), but not in mock-infected DF-1 cells (Fig. 1A). Additionally, we confirmed the rate of infection by flow cytometry (Fig. 1B), which showed that the percentage of IBDV-positive cells was 99.4 ± 0.2% at 24 hpi. These results indicated that 24 hpi would be the best sample collection time

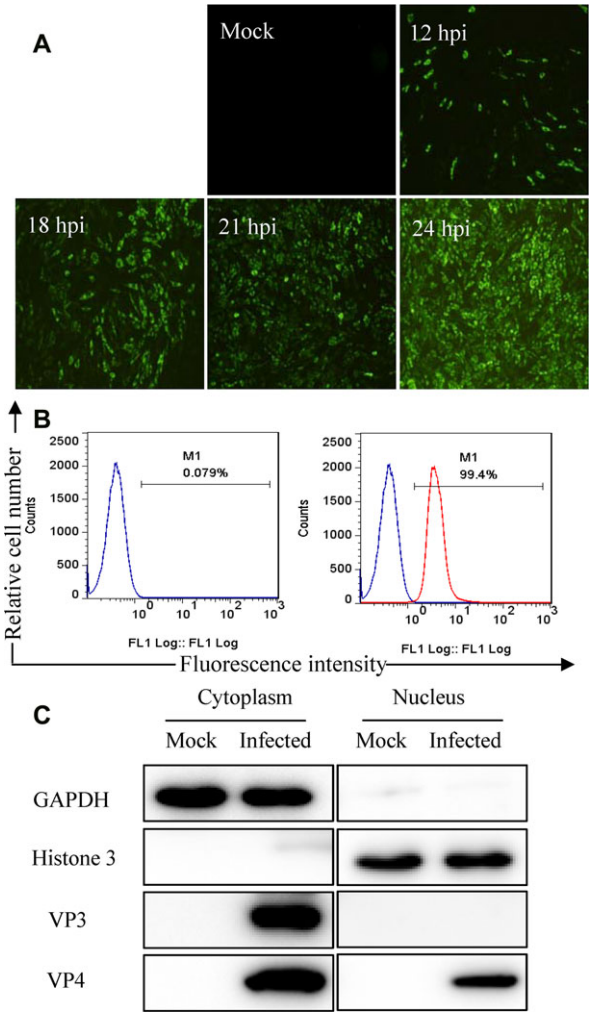

Figure 1. Confirmation of DF-1 cells infected with IBDV. (A) Detection of IBDV in DF-1 cells with IFA. Mock- and IBDV-infected DF-1 cells were collected at 12, 18, 21, and 24 hpi and stained with mAb to IBDV VP3 protein followed by FITC-labeled IgG (green). (B) Quantification of infected cells by flow cytometry. IBDV- and mock-infected DF-1 cells were assayed by single-color flow cytometric analysis. This figure shows the percentage of IBDV-infected cells at 24 hpi. Cells were stained with anti-VP4 mAb labeled with FITC. Mock-infected DF-1 cells served as a negative control (blue line). The mean percentage ± SD of infected cells from a representative experiment performed in triplicate was 99.4 ± 0.2%. (C) Detection of the cytoplasmic and nuclear fractions from IBDV- and mock-infected cells by Western blotting. GAPDH and histone H3 were used as markers of cytoplasmic and nuclear proteins, respectively. IBDV viral proteins VP3 and VP4 were used as markers of infection.

point for iTRAQ analysis. Therefore, cytoplasmic and nuclear fractions were extracted from the cells at 24 hpi. The enrichment of proteins in these two fractions was confirmed by Western blot using GAPDH as a cytoplasmic protein marker and histone 3 as a nuclear protein marker (Fig. 1C). The result showed that the protein markers GAPDH and histone 3 appeared in cytoplasm and nucleus, respectively, indicating the procedure used for cytoplasmic and nuclear fractionation was suitable for iTRAQ analysis.

Table 1. Differentially abundant proteins in IBDV-infected DF-1 cells by iTRAQ analysis. The 57 unique proteins identified

UniProt data protein ID[a)]	Protein name[b)]	Gene symbol	Sequence coverage[c)] (%)	Unique peptides[d)]	p*I*	Ratio[e)]	*t*-Test *p*-value[f)]	Function
Upregulated cytoplasmic proteins								
P18302	Drebrin	DBN1	2.1	1	4.16	2.22	0.00006	Actin binding and profilin binding
F1P3J2	Uncharacterized	IFIT5	2.4	1	5.50	2.00	0.00018	Type I interferon mediated signaling pathway
F1NJ08	Vimentin	VIM	31.3	13	4.85	1.64	0.00001	Integrity of the cytoplasm, immune response
E1C2F2	Pinpin	PNN	1.9	1	6.71	1.58	0.01102	Participates in the regulation of alternative pre-mRNA splicing
F1NEG6	Uncharacterized	hnRNPH1	4.6	3	5.50	1.51	0.00714	mRNA processing
P13648	Lamin A	Lamin A	3.3	2	6.93	1.47	0.01063	Structural molecule activity protein binding
P16039	Nucleophosmin	NPM1	21.4	6	4.39	1.42	0.00008	Transcription coactivator activity
Q9YIC3	FK506-binding protein 9	FKBP	2.8	1	4.76	1.42	0.00302	Peptidyl-prolyl *cis–trans* isomerase activity
F1NZA1	Uncharacterized	TTLL12	3	2	4.84	1.37	0.00084	Cellular protein modification process
Q5F3D2	Uncharacterized	hnRNPH3	9.4	2	7.13	1.33	0.00204	Involved in the splicing process and participates in early heat shock-induced splicing arrest
Q07598	Nonspecific lipid-transfer protein	SCP2	2	1	8.30	1.33	0.00102	Fatty-acyl-CoA binding and receptor binding transfer protein
E1C8Y9	Uncharacterized	SRF3	17.1	3	12.14	1.29	0.03277	mRNA processing and regulating alternative splicing
Q5ZML3	Serine/arginine-rich splicing factor 1	SRSF1	30	8	6.95	1.27	0.00051	mRNA processing and regulating alternative splicing
E1BQK9	Uncharacterized	CUL4B	1.4	1	8.03	1.25	0.02890	Ubiquitin protein ligase binding
Q5F3E8	BTB/POZ domain containing adapter for CUL3-mediated RhoA degradation protein 3	TNFAIP1	4.8	1	7.88	1.25	0.01300	Negative regulation of Rho protein signal transduction
F1NZD3	Uncharacterized	RBMX	11.2	4	10.49	1.23	0.00049	Plays several role in the regulation of pre- and posttranscriptional processes
P09102	Protein disulfide isomerase	PDIA1	12	7	4.42	1.20	0.01984	Protein disulfide oxidoreductase activity
I3VQH4	Interleukin enhancer binding factor 3	ILF3	4.3	1	9.14	1.17	0.0005	Double-stranded RNA binding and RNA binding
H9KZT7	Uncharacterized	NF45	5.9	2	5.10	1.10	0.0459	Double-stranded RNA binding and RNA binding
Downregulated cytoplasmic proteins								
E1C115	Uncharacterized	EIF4EBP1	7.8	1	4.39	0.83	0.00097	Eukaryotic initiation factor 4E binding
Q90ZG0	Peptidyl-prolyl *cis–trans* isomerase	PPIA	25	2	8.48	0.83	0.00057	Mediates ERK1/2 activation
A7UEA7	Multifunctional protein ADE2	PAICS	8.5	4	8.33	0.82	0.00022	Purine nucleobase biosynthetic process
E1BYW9	Proteasome subunit beta type	PSMB3	4.4	1	5.05	0.81	0.00195	Cleave peptides in an ATP/ubiquitin-dependent process in a nonlysosomal pathway
F1NNS8	Uncharacterized	PRDX4	5.2	1	8.57	0.77	0.01341	Activation of the transcription factor NF-kappa B

(Continued)

Table 1. Continued

UniProt data protein ID[a)]	Protein name[b)]	Gene symbol	Sequence coverage[c)] (%)	Unique peptides[d)]	p*I*	Ratio[e)]	*t*-Test *p*-value[f)]	Function
F1NY51	Uncharacterized	UCHL3	10	2	4.64	0.77	0.01857	Catalyze the removal of ubiquitin from polypeptides
Upregulated nuclear proteins								
E1C2Y5	C-C Motif chemokine 4 homolog	CCL4	8.9	4	9.33	1.96	0.00758	Receptor for a C-C type chemokine
E1C8B5	Uncharacterized	KIN	5.6	2	9.49	1.39	0.00504	DNA replication and the cellular response to DNA damage
Q5ZK63	Activated RNA polymerase II transcriptional coactivator p15	TCP4	44.4	3	10.29	1.38	0.00188	Transcription coactivator activity
Q5ZL92	Eukaryotic translation initiation factor 6	EIF6	19.1	11	4.30	1.37	0.00621	Translation initiation factor activity
F1NH66	Uncharacterized	EML4	1.6	1	6.25	1.30	0.00005	May modify the assembly dynamics of microtubules
Q5ZJK3	Signal transducer and activator of transcription	STAT1	12.2	8	5.80	1.26	0.00065	Mediates cellular responses to interferons
F1NZJ2	Uncharacterized	HK1	18.6	1	6.72	1.26	0.03647	Metabolism pathways
F1P222	LDLR chaperone MESD	MESDC2	30.2	7	6.80	1.22	0.00101	Acts as a modulator of the Wnt pathway
E1C214	Ubiquitin carboxyl terminal hydrolase 16 isoform x2	UBP16	1.5	1	5.75	1.22	0.00004	Ubiquitin-specific protease activity
F1NA16	Uncharacterized	SREK1	2.1	1	10.69	1.22	0.03237	Participates in the regulation of alternative splicing
E1BZH9	Uncharacterized	HADH	15.2	5	9.16	1.21	0.00227	Metabolic pathways
E1BVT3	Malate dehydrogenase	MDH2	52.5	16	8.73	1.21	0.00038	Operates in the metabolic coordination between cytosol and mitochondria
F1NR57	Uncharacterized	SLC2A11	1.9	2	6.89	1.20	0.00054	Facilitative glucose transporter
O93257	X-ray repair cross-complementing protein	XRCC6	9.2	5	6.02	1.20	0.03621	ssDNA-dependent ATP-dependent helicase
E1BZJ3	Uncharacterized	NPL4	8.9	4	6.34	1.11	0.0075	Protein binding and zinc ion binding
Q5ZMW3	Apoptosis inhibitor	API5	44.4	3	7.45	1.10	0.0071	Inhibiting apoptosis
Downregulated nuclear proteins								
F1NRD9	ATP-dependent RNA helicase	DDX1	19.5	11	6.89	0.93	0.0291	Enhance NF-kappa B mediated transcriptional activation
E1C2E3	Uncharacterized	VDAC3	20.5	6	9.25	0.85	0.0500	Porin activity and nucleotide binding
F1NPD3	60S ribosomal protein l18a	RPL18A	17	3	11.40	0.83	0.00034	Structural constituent of ribosome and RNA
Q5ZMD0	Uncharacterized	NOP56	6.2	3	9.65	0.82	0.00327	Involved in the early to middle stages of 60S ribosomal subunit biogenesis
F1NC34	Uncharacterized	SLC35B2	4.9	2	9.33	0.82	0.01273	May indirectly participate in activation of the NF-kappa B and MAPK pathways
P53449	Fructose-bisphosphate aldolase C	ALDOC	35.8	3	6.51	0.82	0.00034	Glycolytic enzymes
A0M8T8	Caveolin-1	CAV1	24.2	4	6.23	0.82	0.02114	Structural molecule activity and receptor binding activity and receptor binding

(Continued)

Table 1. Continued

UniProt data protein ID[a)]	Protein name[b)]	Gene symbol	Sequence coverage[c)] (%)	Unique peptides[d)]	p*I*	Ratio[e)]	*t*-Test *p*-value[f)]	Function
Q5ZJZ5	D-Beta-hydroxybutyrate mitochondrial	BDH1	3.2	1	9.58	0.82	0.01216	Phospholipid binding and 3-hydroxybutyrate dehydrogenase activity
E1C6C9	Uncharacterized	NDUFB10	12	2	6.27	0.82	0.03815	NADH dehydrogenase (ubiquinone) activity
Q7T2Z7	Collagen alpha-1 chain	COL1A1	3.8	1	7.47	0.81	0.00414	Cell growth and repair
Q5ZMF9	Uncharacterized	DERL1	4.4	1	9.58	0.81	0.01588	Participate in the endoplasmic reticulum associated degradation response
P22451	60S ribosomal protein l5	RPL5	22.9	7	10.22	0.80	0.00758	RNA binding
P61355	60S ribosomal protein l27	RPL27	18.4	3	11.23	0.80	0.01773	Structural constituent of ribosome
F1N9I7	Probable carboxypeptidase pm20d1	PM20D1	1.5	1	7.22	0.79	0.04083	Metabolic process
F1P0H9	Collagen alpha-2 (I) chain	COL1A2	26.8	25	9.68	0.79	0.01093	Cell growth and repair
F1NH93	Uncharacterized	RPS20	19.7	2	10.71	0.77	0.00008	Structural constituent of ribosome and RNA binding
Q5F491	Uncharacterized	DDX42	22	11	6.99	0.77	0.0004	RNA binding and ATP-dependent helicase activity
Q2MCJ7	Aquaporin-1	AQP1	7.4	1	6.91	0.76	0.00052	Water channel activity and transporter activity
F1NFE0	Collagen alpha-1(VI) chain	COL6A1	18.1	14	5.65	0.76	0.01548	Acts as a cell-binding protein
F1NJT3	Fibronectin	FINC	16.1	34	5.34	0.74	0.00113	Involved in cell adhesion and migration processes
P15988	Collagen alpha-2 (VI) chain	COL6A2	16.9	16	5.61	0.74	0.00006	Acts as a cell-binding protein
P02457	Collagen alpha-1 (I) chain	COL1A1	45.6	45	5.21	0.73	0.00004	Cell growth and repair

a) Protein IDs according to UniProt.
b) Protein name of the proteins identified by iTRAQ with LC-MS/MS.
c) Percent sequence coverage of identified proteins.
d) Number of unique peptides identified for each protein (in three independent biological replicates).
e) Ratios of IBDV-infected/mock-infected.
f) *p*-Value of significant index.

3.2 Protein profiling by iTRAQ coupled LC-MS/MS analysis

Protein identification and quantification from cytoplasmic fraction and nuclear fraction were performed, respectively, using 6-plex iTRAQ labeling combined with LC-MS/MS analysis. Two fractions iTRAQ sample sets were analyzed, including three independent biological replicates of cytoplasmic and nuclear fractions (Supporting Information Fig. 1). Based on the LC-MS/MS data, 1152 and 2117 proteins were identified from the cytoplasmic and nuclear cell fractions, respectively. Of the identified proteins, we reliably quantified 3211 proteins, of which 23 and 34 proteins were differentially abundant proteins in the cytoplasmic and nuclear fractions (fold changes ≥ 1.2 or ≤ 0.83) as a result of infection [26], respectively (Table 1, Fig. 2A). However, of 57 identified proteins, 19 proteins were identified by one unique peptide from three biological replicates, the MS/MS spectrum for each of these proteins are included in Supporting Information Fig. 2. In addition, these differentially abundant proteins were clustered hierarchically with Cluster 3.0 software (Fig. 2B). Based on this analysis, these proteins were found to belong to two groups where the amount of protein increased and decreased at 24 hpi in the cytoplasmic and nuclear fractions, respectively.

3.3 Bioinformatics analysis of differentially abundant proteins

In order to understand our proteomic profiles, the identified and quantified proteins were analyzed further by different bioinformatic tools. The numbers of proteins for different subcellular location were quantified using the gene ontology

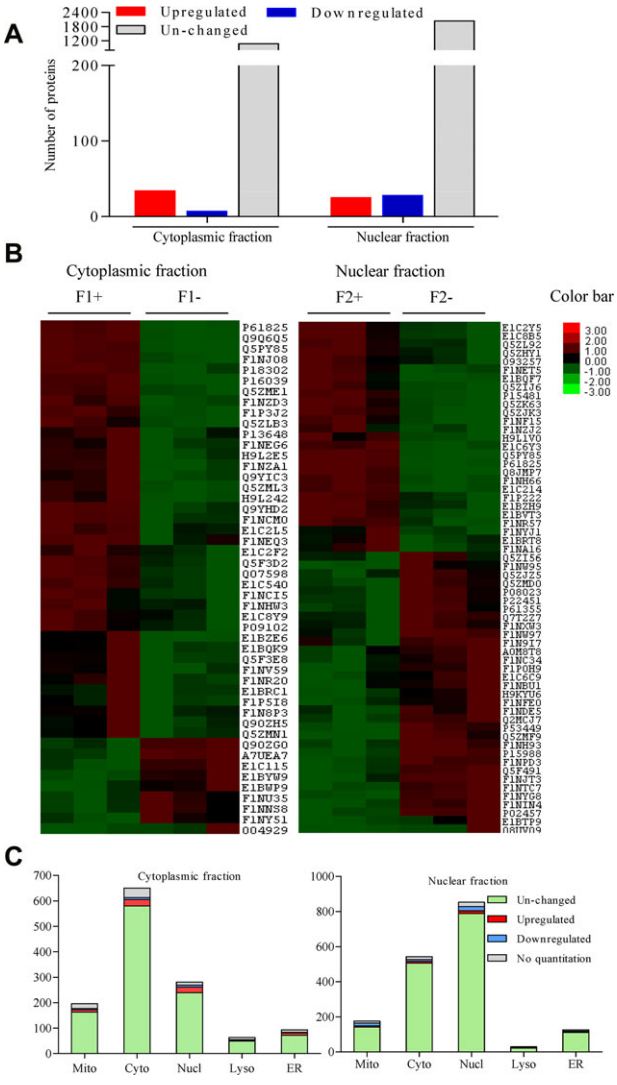

Figure 2. Statistical analysis of quantitative subcellular proteomic data from IBDV-infected DF-1 cells. (A) Quantitative analysis using numbers of differentially abundant proteins in cytoplasmic and nuclear fractions. (B) Hierarchical cluster analysis for differentially abundant proteins in cytoplasmic and nuclear fractions. Differentially abundant proteins are shown with a pseudo-color scale (from −3 to 3) indicating high (red) and low (green) abundance. (C) Classification of proteins in different fractions using gene ontology. All identified proteins in cytoplasmic, nuclear, lysosomal, mitochondrial, and endoplasmic reticulum were annotated.

(GO) annotations (Fig. 2C). It can be seen that cytoplasmic localization of proteins annotated was the largest proportion in the cytoplasmic fraction. Similarly, nuclear proteins were most abundant in the nuclear fraction. Additionally, some proteins showed cytoplasmic annotation using our dataset also appeared in the nuclear fraction. Thus, some proteins apparently had shifted between the nucleus and cytoplasm after IBDV infection.

Simultaneously, to better understand the implications of host responses to IBDV infection, we analyzed the differentially abundant proteins with the "biological process" GO annotation. Shown in Fig. 3, about half of the proteins are involved in regulation of cellular, metabolic, and biological processes. Based on the statistical analysis of cytoplasmic proteins, the cell proliferation, developmental process, multicellular organismal process, and locomotion were identified in the upregulated proteins (Fig. 3A, in red), indicating that these processes were more active inside the cytoplasm after IBDV infection. Interestingly, these processes were found in the downregulated nuclear fraction (Fig. 3B, in red), but not in the upregulated nuclear fraction. The above data showed a dynamic shift of differentially abundant proteins between the cytoplasm and nucleus.

3.4 Assessment of mRNA transcript

We assessed the mRNA abundance of 25 identified proteins by quantitative real-time RT-PCR (Fig. 4). These proteins had differentially abundant in MS/MS. The *GAPDH* mRNA transcript was used as a control housekeeping gene. In general, most of the change trends of 25 mRNA were similar to their proteins in iTRAQ analysis (Table 1). Among these genes, the abundance of the innate immune associated genes *IFIT5* [27] and *STAT1* were evidently increased, while the genes eukaryotic translation initiation factor 4E binding protein 1 (*EIF4EBP1*), DEAD-box RNA helicase 1 (*DDX1*), and DEAD-box RNA helicase 42 (*DDX42*) were decreased. Transcriptional levels of chemokinetic and inflammatory associated genes c-c motif chemokine 4 homolog (*CCL4*) and FK506 Binding Protein (*FKBP*) were increased. Similarly, metabolic process and signaling associated genes *hnRNPH1*, interleukin enhancer-binding factor 3 (*ILF3*), *NPL4*, and *NF45* were also increased, but the transcription of antioxidant enzyme gene peroxiredoxin 4 (*PRDX4*) was decreased in abundance. Additionally, although the mRNA level of apoptosis inhibitor associated gene *API5* was increased, that of the voltage-dependent anion channel 3 (*VDAC3*) gene was decreased. A variety of factors can affect gene expression. In this study, changes in mRNA of most genes were consistent with its corresponding protein abundance, which indicated these proteins may be regulated at the mRNA level.

3.5 Validation of changes in protein levels for differentially abundant proteins

To provide additional evidence to validate the differentially abundant proteins identified by the iTRAQ-labeled LC-MS/MS system, five proteins in both the cytoplasmic and nuclear fractions (IFIT5, hnRNPH1, NF45, API5, and STAT1) were detected by Western blot analysis (Fig. 5). GAPDH and histone 3 were used as the marker and loading controls of cytoplasmic and nuclear proteins, respectively. The significant increases of IFIT5 were observed in the cytoplasmic fractions of IBDV-infected cells. The abundance

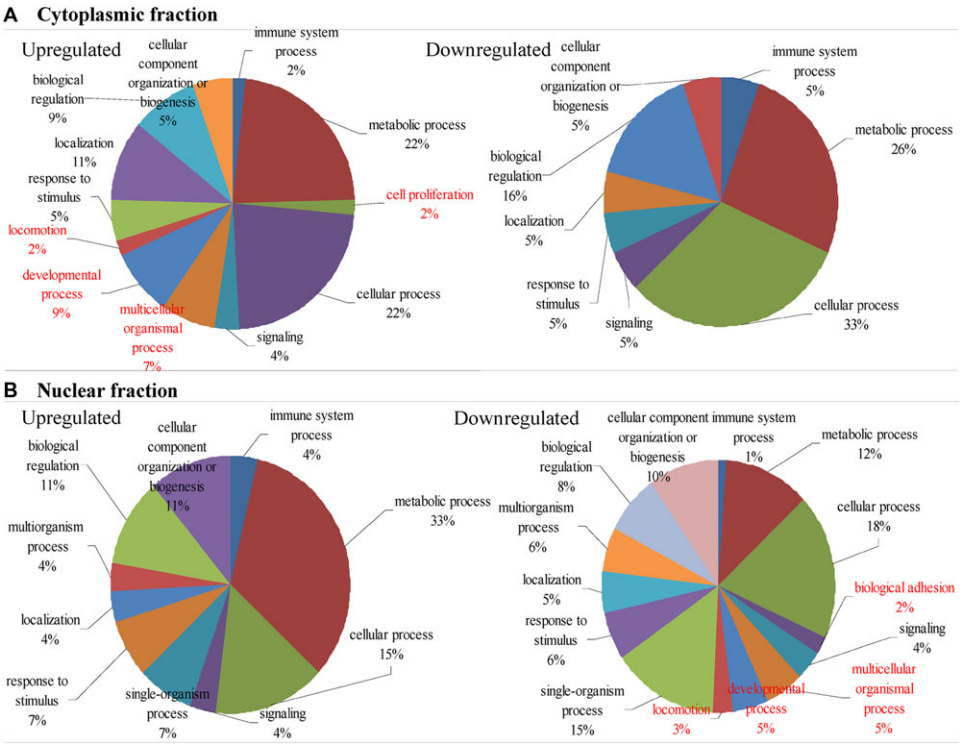

Figure 3. Biological processes analysis of differentially abundant proteins based on gene ontology. (A) Relative proportions of various proteins that were increased or decreased in abundance in the cytoplasmic fraction. (B) Relative proportions of various proteins that were increased or decreased in abundance in the nuclear fraction. Percentages of protein numbers in each category are displayed in brackets.

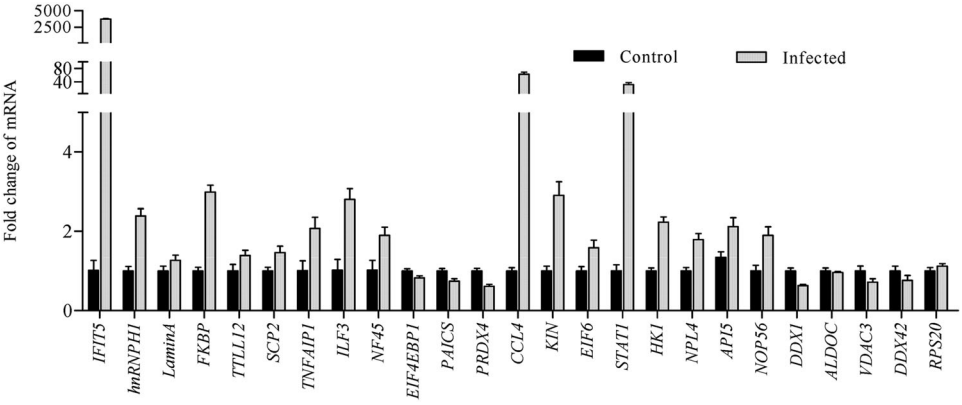

Figure 4. Transcriptional profiling of differentially abundant proteins in IBDV-infected DF-1 cells. The mRNA changes of IBDV-infected cells was detected by real-time RT-PCR. All samples were normalized to the *GAPDH* gene as a control. The fold increase or decrease was relative to mock-infected cells as the reference. Error bars represent SDs.

of the nuclear STAT1 protein was identified as increase in the nuclear fractions by MS analysis, and the Western blot results supported this observation. The API5 protein was shown to be nonsignificantly increased in abundance in the nucleus of IBDV-infected cells compared with mock-infected cells, which was consistent with the MS results. However, the intracytoplasmic API5 protein was significantly increased in abundance, which was not found in the MS analysis. Significant increases of NF45 and hnRNPH1 were observed in the cytoplasmic fraction of IBDV-infected cells. Interestingly, NF45 mostly appeared in the nucleus, but then shifted to the cytoplasm after IBDV infection. Generally, except for API5, the change trends in protein abundance of other four proteins were similar to the change patterns of their corresponding proteins in iTRAQ analysis.

3.6 Colocalization of viral protein VP3 with host protein

Confocal microscopy can be used to monitor not only the subcellular localization of proteins, but also changes in protein abundance [28]. Thus, several quantitative proteomics studies have employed confocal microscopy to validate their MS results [25, 29]. In our study, colocalization analysis was performed by the double staining indirect immunofluorescence assay (IFA) analysis using the pAbs to NF45, hnRNPH1, DDX42, NPL4, and API5, and the mAb to VP3 protein of IBDV. In mock-infected cells (Supporting Information Fig. 3), hnRNPH1, API5, and NPL4 were mainly expressed in the cytoplasm, while NF45 and DDX42 appeared in the nucleus. Distribution patterns of

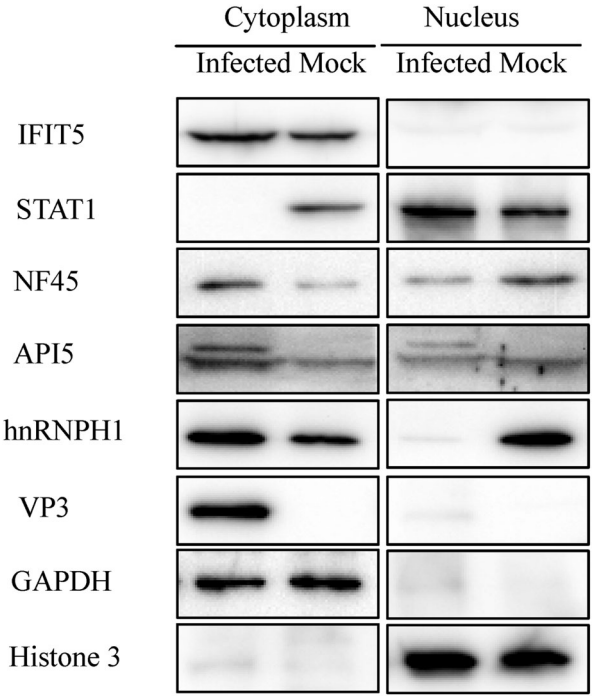

Figure 5. Western blot analysis of selected differentially abundant proteins in cytoplasmic and nuclear fractions of IBDV-infected cells. The differentially abundant proteins NF45 was increased in the cytoplasmic fraction and translocated from nucleus to the cytoplasm upon virus infection. Equal amounts of protein fractions were loaded, and the abundance of IFIT5, hnRNPH1, NF45, API5, STAT1, and viral protein VP3 were determined using specific pAbs/mAbs. Mock-infected cells were used as a negative control. GAPDH and histone 3 were used as the marker and loading control for the cytoplasm and nucleus, respectively.

the above-mentioned cytoplasmic proteins in IBDV-infected cells were the same as those in mock-infected cells, but the fluorescence intensities of these proteins were increased in infected cells compared with mock-infected cells. In IBDV-infected cells at 24 h after inoculation, the VP3 viral protein signal overlapped with that of NF45, hnRNPH1, DDX42, NPL4, and API5 (Fig. 6). Interestingly, NF45 and DDX42, which are normally expressed in the nucleus, were colocalized with the viral protein VP3 in the cytoplasm of IBDV-infected cells, indicating that NF45 and DDX42 were translocated from the nucleus to cytoplasm during infection. Moreover, the abundance of NF45 clearly increased and accumulated in the cytoplasm of IBDV-infected cells.

3.7 Network analysis of differentially abundant proteins

We constructed the pathways of differentially abundant proteins by canonical pathway analysis. For the pathway analysis, 11 canonical pathways were affected significantly during IBDV infection ($p \leq 0.05$). As shown in Fig. 7A, telomere extension by telomerase ($p = 3.51 \times 10^{-4}$, ratio 0.111) was the top priority in the cytoplasmic proteome, other favored the role of p14/p19ARF in tumor suppression ($p = 1.43 \times 10^{-3}$, ratio 0.057) and inosine-5′-phosphate biosynthesis II ($p = 5.6 \times 10^{-3}$, ratio 0.062). Meanwhile, the ratio in telomere extension by telomerase pathway showed the most significant among the ten canonical pathways. Additionally, the nuclear proteome (Fig. 7B) tended to heavily favor eIF2 signaling as the primary pathway ($p = 1.09 \times 10^{-4}$, ratio 0.025), which is highly conserved and vitally important for antiviral responses [30]. Other significant associations included gluconeogenesis I, intrinsic prothrombin activation pathway, and mitochondrial dysfunction (Fig. 7B).

In order to determine how IBDV interacts with the host proteins and how they affect cellular functions, we constructed virus–host interaction networks by IPA. Network maps of both cytoplasmic proteins and nuclear proteins were created (Fig. 8A and B). For the network analysis, cytoplasmic proteins involved in RNA posttranscriptional modification, molecular transport, and RNA trafficking were grouped together (Fig. 8A). Most of the cytoplasmic proteins were linked to the mTOR signaling, ERK/MAPK signaling, and protein ubiquitination pathways. Additionally, in the nuclear fraction, proteins involved in DNA replication, repair, cell-mediated immune response, and cellular development were grouped together (Fig. 8B). The bioinformatic analysis suggests that the PI3K/Akt signaling pathway and IFN-β signaling cascades are vitally involved in IBDV infection. Certain proteins increased in abundance in infected cells are known to be products of IFNs, such as IFIT5 [27,31] and STAT1 [32,33], which implies a specific antiviral response in the host cells. Due to limitations of the database or unknown functions of the host protein, some of the differentially abundant proteins were not included in this network.

4 Discussion

Reliable quantitative methods are essential in biomarker discovery and to interpret proteomic data. In recent years, subcellular prefractionation has been employed as a popular technique to reduce sample complexity, extend protein coverage, and more critically, to provide a spatial description of proteins in the cell. Understanding virus–host interactions is critical for elucidating molecular mechanisms associated with functional alterations of IBDV-infected cells. Until now, no study had examined the subcellular proteome of IBDV-infected cells, although proteomic analyses of in vitro IBDV-infected CEFs [6] and in vivo IBDV-infected bursa of Fabricius [9] from our research group were previously reported. In the current work, we used a subcellular iTRAQ proteomic approach to characterize differentially abundant proteins in the cytoplasmic/nuclear fractions of IBDV-infected DF-1 cells. Comparative analysis of the results by MS revealed that in the cytoplasmic proteome of virus-infected cells, altered cellular proteins included 17 increased proteins

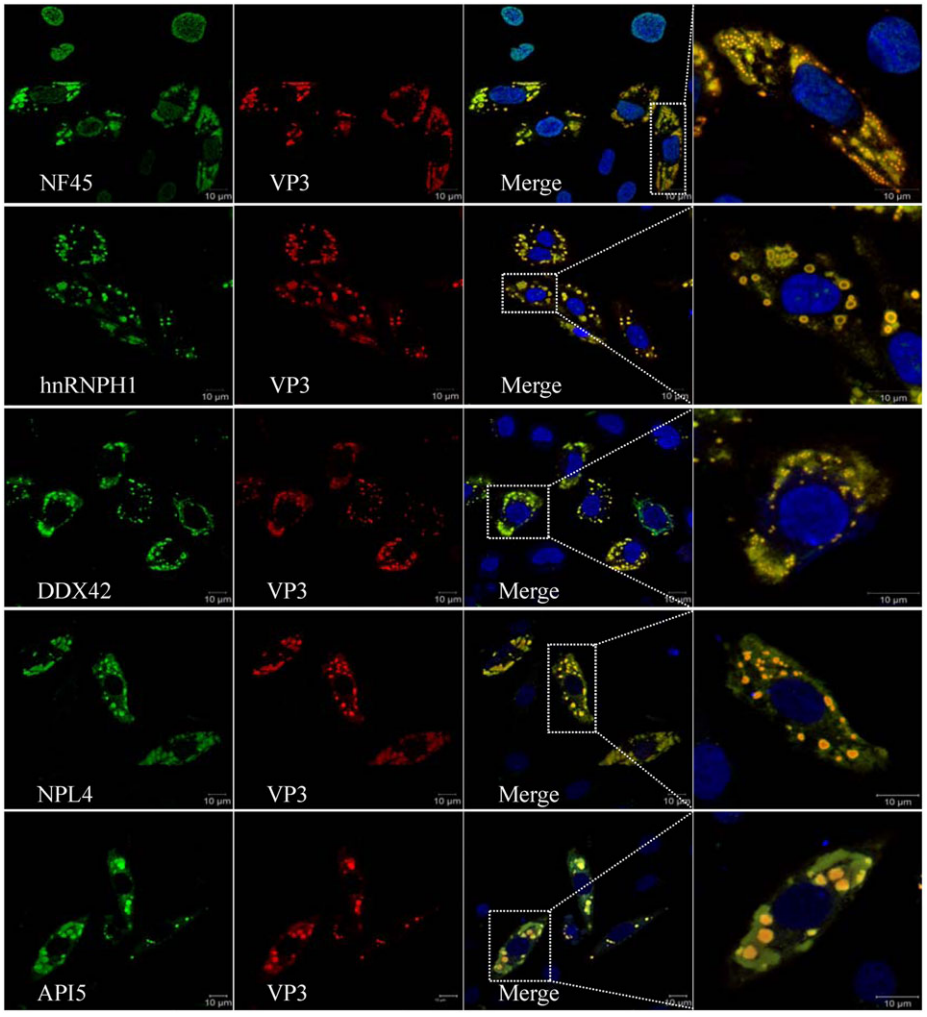

Figure 6. Immunofluorescence analysis of subcellular distribution of cellular NF45, hnRNPH1, DDX42, NPL4, and API5 with IBDV VP3 protein by confocal microscopy. IBDV-infected DF-1 cells reacted with anti-VP3 mAb and anti-hnRNPH1, anti-NF45, anti-API5, anti-NPL4, or anti-DDX42 pAbs as a primary antibody, followed by the FITC-conjugated (green) goat/rabbit IgG and Alexa Fluor 546 conjugated (red) mouse IgG. The fixed cell nuclei were stained with DAPI (blue).

in abundance and six decreased proteins in abundance. In the nuclear proteome, 34 altered cellular proteins were identified, including 14 increased proteins in abundance and 20 decreased proteins in abundance. Additionally, IFA showed the interplay between the viral protein VP3 and cellular protein NF45. Clearly, further studies are necessary to understand the roles of the altered cellular proteins in IBDV infection. Possible biological functions and pathways associated with these differentially abundant proteins were explored by the IPA package, and the identified cellular proteins were found to be mainly involved in immune system process, biological regulation, molecular transport, signaling, and metabolic process.

In present study, except for that two altered proteins were found identical in IBDV-infected CEF cells by 2DE and iTRAQ, we also found that most of the differentially increased proteins in abundance were different in comparison with our previous research reports using 2DE [6, 9]. We identified more cytosolic and nuclear proteins with iTRAQ-based quantitative subcellular proteomics. Proteins not identified in previous 2DE proteomics included IFIT5, NF45, STAT1, and API5 involved in immune response and cellular apoptosis. Apart from this, RNA processing and energy metabolism related proteins hnRNP H1, DDX42, and DDX1 also were supplemented from our data. Generally, the iTRAQ method provided the finer details of the subcellular proteome of IBDV-infected cells, and more information for different compartments of host cells. To our knowledge, this study is the first to report a subcellular proteomic analysis of the response to IBDV infection.

IFIT genes encode a family of proteins that are induced after IFN treatment, viral infection, or PAMP recognition [34]. IFIT proteins are poised to confer inhibitory effects after infection, and they have been found to be increased in abundance in target cells infected with various viruses, such as H3N2 swine influenza virus [11], Japanese encephalitis virus (JEV) [35], and porcine reproductive and respiratory syndrome virus [16]. Recently, progress was made in identifying how IFIT proteins inhibit through distinct mechanisms of action, and the replication of multiple families of viruses [36], such as hepatitis C virus [37], influenza A virus, and vesicular stomatitis virus [38]. One of the IFIT family genes, *IFIT5* (*ISG58*), is involved in anti-viral responses through enhancing innate immune signaling pathways [27]. In the present study, IFIT5 was revealed to be increased in

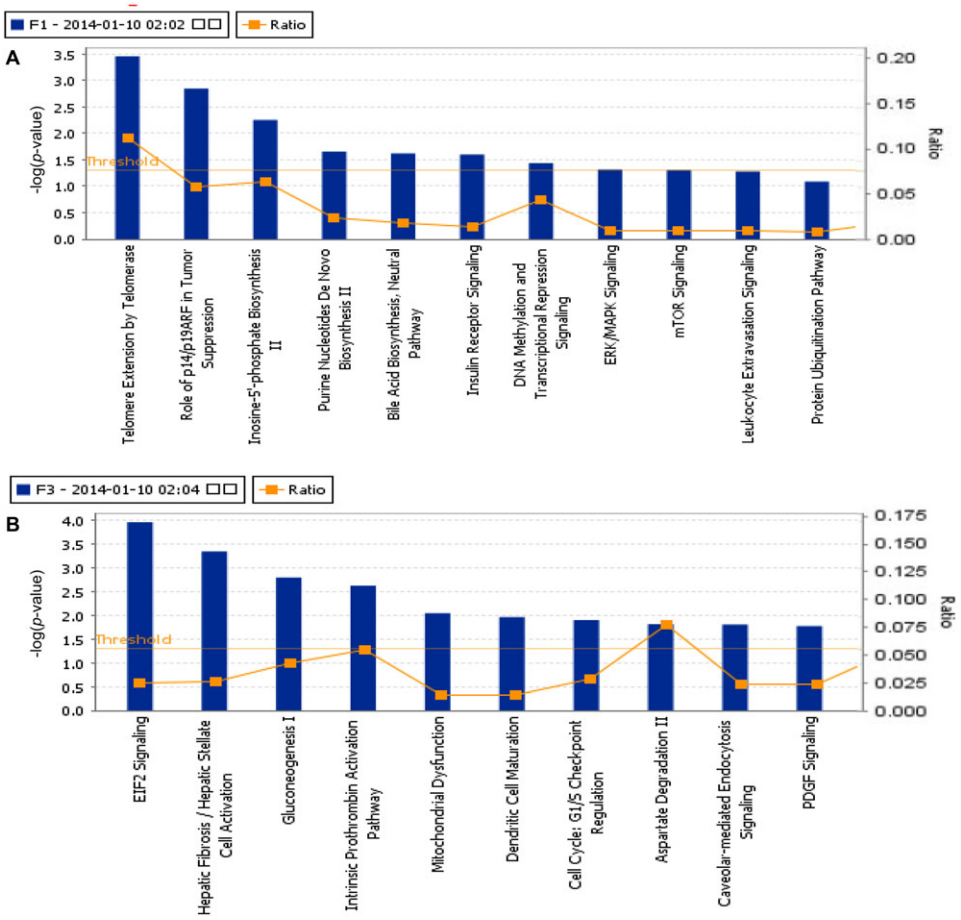

Figure 7. Signaling pathways in subcellular fractions significantly affected by virus infection. (A) Top 11 signaling pathways in the cytoplasmic proteome. (B) Top 10 signaling pathways in the nuclear proteome. Cononical pathway analysis were conducted by IPA software. The pathway involved was shown by *p*-value of regulated proteins. The ratio represented that number reached threshold criteria divided total number of the given pathway.

abundance during IBDV infection (increased ~2.001-fold in the cytoplasmic fraction). Therefore, it is conceivable that IFIT5 may be an important modulator in the antivial innate immune response during IBDV infection. STAT1 is a downstream target of the IFN pathway, which is central to the regulation of immune responses in viral invasion. Type I IFN binds to a common IFN-α/β receptor that initiates a signaling cascade that results in the phosphorylation and nuclear translocation of STAT1 and the induction of the expression of hundreds of IFN-stimulated genes [33, 39]. In the present study, STAT1 was notably upregulated during IBDV infection. However, the upregulated mechanism of STAT1 needs further investigation in IBDV-infected DF-1 cells.

Our analysis found increased abundance of the RNA processing and translation-associated gene *hnRNPH1* in the cytoplasmic fraction of IBDV-infected cells. As RNA binding proteins, hnRNPs are associated with pre-mRNAs in the nucleus and appear to influence pre-mRNA processing and other aspects of mRNA metabolism and transport [40–42]. Previous reports have shown that poliovirus infection cause redistribution of the cellular hnRNPs A1 and K from the nucleus to the cytoplasm [43], and hnRNP U is colocalized with vesicular stomatitis virus [44]. HnRNP H1 has also been implicated in assisting hepatitis C virus replication [41]. Moreover, confocal microscopy analysis showed colocalization of hnRNP H1 protein with the viral protein VP3 in the cytoplasm of IBDV-infected cells (Fig. 6B). VP3 has multiple functions that contribute to efficient virus replication [45]. Therefore, we hypothesized that the increased abundance of hnRNP H1 may play an important role in the replication of IBDV. Among the differentially abundant proteins, we also found decrease in abundance of cellular proteins associated with RNA processing and biosynthesis, including 60S ribosomal protein l5 (RPL5, for RNA binding) and malate dehydrogenase 2 (MDH2, operates the metabolic coordination between cytosol and mitochondria). Notably the proteomic data further revealed that the key glycolytic enzymes, including aldolase C (ALDOC), were extensively decreased in abundance. Based on these proteomic analyses, we speculate that IBDV replication may extensively inhibit the host cellular metabolic pathways involved in glycolysis and energy metabolism as well as mRNA processing.

We also found differentially abundant proteins associated with DEAD-box RNA helicases DDX1 and DDX42 (Fig. 6), which are involved in many aspects of RNA metabolism. Additionally, DDX1 was shown to be an RNA-activated ATPase, wherein Rev-bound RNA was equally effective at stimulating ATPase activity as protein-free RNA. DDX1 interacted with HIV-1 Rev and involved in virus replication in Hela cells [46]. Moreover, DDX1 interacted with

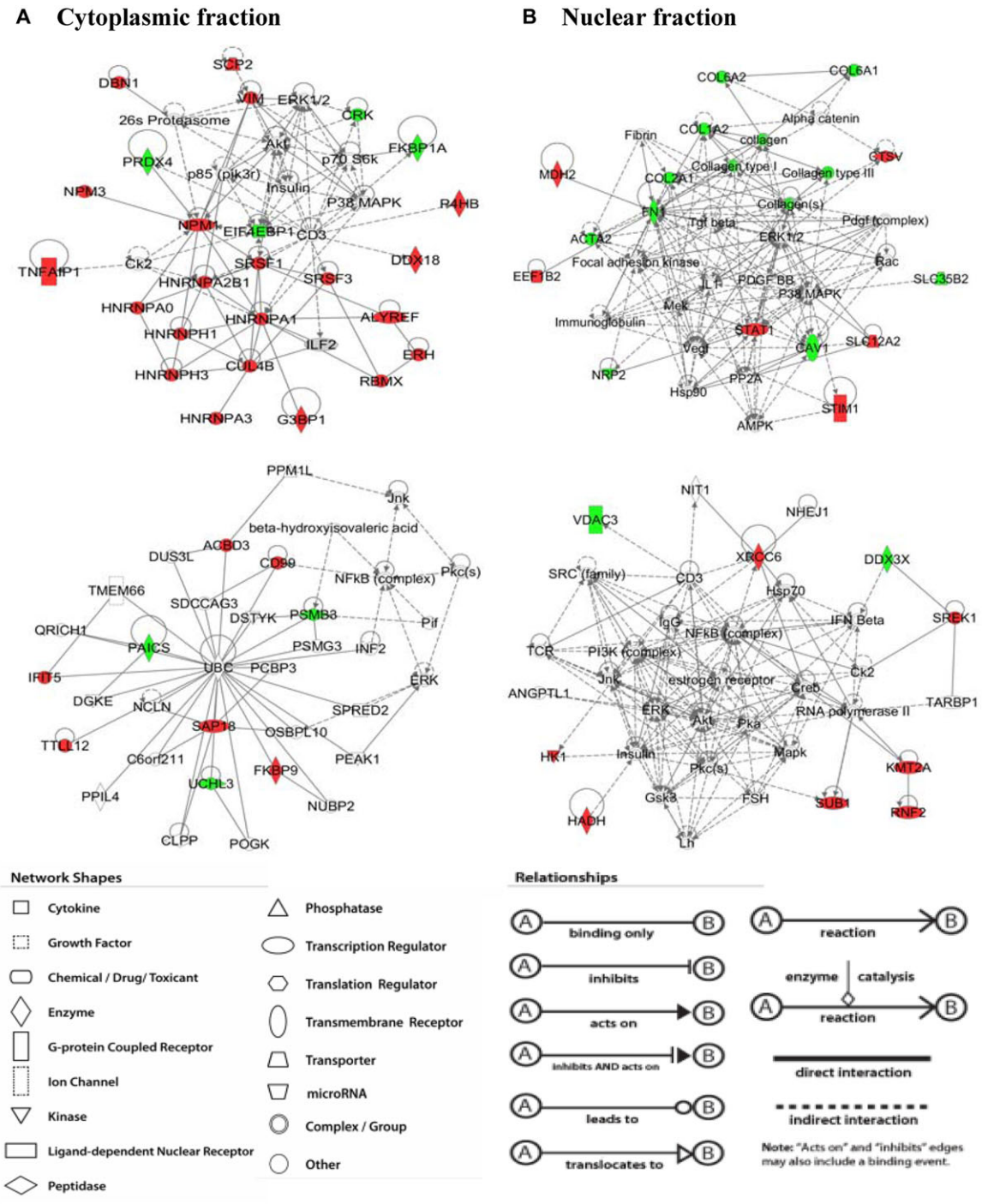

Figure 8. Analysis of interaction network pathway for identified proteins in cytoplasmic fraction (A) and nuclear fraction (B). Proteins that were found to be increased or decreased in abundance in the cytoplasmic or nuclear fraction were submitted to network analysis using Ingenuity Systems. Green color indicated proteins showing 0.83 or greater decrease in abundance, and red color showing 1.2 or greater increase in IBDV-infected cells. Different shapes represented different functional class of the proteins. Solid lines and dashed lines indicated, respectively, direct or indirect molecular interaction.

NF-κB subunit RelA (p65) and took part in regulating NF-κB-mediated regulatory pathway [47]. Futhermore, the study found that DDX1 interacted with nsp14 from both coronavirus infectious bronchitis virus (IBV) and severe acute respiratory syndrome coronavirus (SARS-CoV). Intranuclear DDX1 was translocated to cytoplasm in IBV-infected Vero cells. In other words, DDX1 was conducive to enhance coronavirus replication [48]. ATP-dependent RNA helicase DDX42

interacted with JEV NS4A in vitro and in vivo. Importantly, the expression of DDX42 inhibited the confrontation of the response to IFN-β by JEV [49]. Together, these results provided insight into the understanding of IBV pathogenesis.

NF45, also known as ILF2, has been indicated to act as an important regulatory factor involved in transcription, microRNA processing, nuclear export of RNAs, and post-transcriptional and translational regulation of gene expression [50–52]. NF45/NF90 heterodimeric protein complex have involved multitudinous functions, one of the functions was transferred from the nuclear to the cytoplasm in many different cell types [53]. In the infected DF-1 cells, we found predominantly the NF45 protein in the cytoplasmic fraction (Fig. 6). In addition, we also found that NF45 colocalized with VP3 and translocated from the nucleus to cytoplasm during IBDV infection (Fig. 6). This observation was similar to a previous observation of IBDV infection at 12 hpi [54] and consistent with the conclusion that the cytoplasmic accumulation of NF45 as a consequence of the viral infection occurs independently from the expression of IFN-regulated genes.

Some proteins associated with cell death and apoptosis, such as API5, was identified as being altered by IBDV infection. API5 is an antiapoptotic protein that is increased in abundance in various cancer cells, the roles of API5 may be to mediate protein–protein interactions [55]. Morris et al. [56] reported that API5 play an important role in dE2F1-induced apoptosis. Proviral integration of moloney virus-2 can activate API5 through phosphorylation mechanism in order to inhibit the apoptosis of liver cells, and NF-κB is the key regulator in this antiapoptotic pathway [57]. The antioxidant stress protein PRDX4 was decreased in abundance, suggesting that IBDV-infected inhibits host cell oxidative stress. Virus-induced oxidative stress is associated with the activation of phagocytosis and the release of reactive oxygen that positively modulate the immune activation and eradicate viral infection and immune-induced cellular injury [58]. Moreover, Tavender et al. [59] found that PRDX4, an endoplasmic reticulum localized peroxiredoxin and known to play an important role in disulfide formation, can be associated with the endoplasmic reticulum stress response.

In addition, among the differentially abundant proteins, we identified nucleolar protein nucleophosmin 1 (NPM1) in the cytoplasmic fraction. NPM1 has been linked to a variety of important cellular processes, both in and out of the nucleolus, including ribosome processing, molecular chaperoning, maintenance of genomic integrity, centrosome duplication, and transcriptional regulation [60, 61]. It has been reported to function as a chaperone in the viral chromatin assembly process in infected cells [62]. This shuttling of proteins between the nucleus and cytoplasm is now recognized as a key mechanism for ensuring proper cell cycle progression [63]. In previous report, others have identified NPM as a novel p53-independent target of the ARF tumor suppressor protein [64]. Our investigation demonstrated an increased level of NPM1 in IBDV-infected DF-1 cells, which can be hypothesized as an attempt by the host to arrest viral replication inside the cells.

As demonstrated in this study, we first use iTRAQ subcellular proteomic analysis to understand DF-1 cell responses of IBDV infection. Using accurate methods, a total of 57 cellular proteins that were significantly altered postinfection were identified. These data provide clues to elucidate the molecular mechanisms of the interaction between IBDV and target cells.

The MS proteomics data have been deposited to the ProteomeXchange Consortium [65] via the PRIDE partner repository with the dataset identifier PXD001869. This work was supported by grants from China Agriculture Research System (grant no. CARS-41-K11), National Key Technology R & D Program of China (grant no. 2015BAD12B01), and the Priority Academic Program Development of Jiangsu Higher Education Institutions. The authors thank Jianwen Hu (Shanghai Applied Protein Technology Co., China) for help with LC-MS/MS. Besides, they are grateful to Yang Zhang for kindly providing the protein network (Institutes of Biomedical Sciences, Fudan University).

The authors declare no conflict of interest.

5 References

[1] Saif, Y. M., *Vet. Immunol. Immunopathol.* 1991, *30*, 45–50.

[2] Delma, B., Kibenge, F. S., Leong, J. C., Mundt, E., Vakharia, V. N., Wu, J. L. (Eds.), *Birnaviridae*, Academic Press, London 2005, pp. 561–569.

[3] Wong, R. T., Hon, C. C., Zeng, F., Leung, F. C., *J. Gen. Virol.* 2007, *88*, 1785–1796.

[4] Bourchookarn, A., Havanapan, P. O., Thongboonkerd, V., Krittanai, C., *Biochim. Biophys. Acta* 2008, 1784, 504–511.

[5] Liu, N., Song, W., Wang, P., Lee, K., Chan, W., Chen, H., Cai, Z., *Proteomics* 2008, *8*, 1851–1858.

[6] Zheng, X. J., Hong, L. L., Shi, L. X., Guo, J. Q., Sun, Z., Zhou, J. Y., *Mol. Cell. Proteomics* 2008, *7*, 612–625.

[7] Zhang, H., Guo, X., Ge, X., Chen, Y., Sun, Q., Yang, H., *J. Proteome Res.* 2009, *8*, 3091–3097.

[8] Zhang, X., Zhou, J. Y., Wu, Y. P., Zheng, X. J., Ma, G. P., Wang, Z. T., Jin, Y. L., He, J. L., Yan, Y., *J. Proteome Res.* 2009, *8*, 5111–5119.

[9] Wu, Y. P., Peng, C. E., Xu, L., Zheng, X. J., Liao, M., Yan, Y., Jin, Y. L., Zhou, J. Y., *Proteomics* 2012, *12*, 1844–1859.

[10] Zhang, J. Y., Wu, X. P., Zan, J., Wu, Y. P., Ye, C. J., Ruan, X. Z., Zhou, J. Y., *J. Virol.* 2013, *87*, 7608–7621.

[11] Wu, X. P., Wang, S. Y., Yu, Y., Zhang, J. Y., Sun, Z. Y., Yan, Y., Zhou, J. Y., *Proteomics* 2013, *13*, 3309–3326.

[12] Wu, Y. P., Jin, Y. L., Pan, W., Ye, C. J., Sun, X. Y., Sun, Y. T., Hu, B. L., Zhou, J. Y., *Electrophoresis* 2014, *35*, 1130–1143.

[13] Munday, D. C., Surtees, R., Emmott, E., Dove, B. K., Digard, P., Barr, J. N., Whitehouse, A., Matthews, D., Hiscox, J. A., *Proteomics* 2012, *12*, 666–672.

[14] Ross, P. L., Huang, Y. L. N., Marchese, J. N., Williamson, B., Parker, K., Hattan, S., Khainovski, N., Pillai, S., Dey, S., Daniels, S., Purkayastha, S., Juhasz, P., Martin, S., Bartlet-Jones, M., He, F., Jacobson, A., Pappin, D. J., *Mol. Cell. Proteomics* 2004, *3*, 1154–1169.

[15] Liu, J., Bai, J., Lu, Q., Zhang, L., Jiang, Z., Michal, J. J., He, Q., Jiang, P., *J. Proteomics* 2013, *79*, 72–86.

[16] Lu, Q., Bai, J., Zhang, L. L., Liu, J., Jiang, Z. H., Michal, J. J., He, Q. D., Jiang, P., *J. Proteome Res.* 2012, *11*, 2890–2903.

[17] Linde, M. E., Colquhoun, D. R., Mohien, C. U., Kole, T., Aquino, V., Cotter, R., Edwards, N., Hildreth, J. E. K., Graham, D. R., *J. Proteome Res.* 2013, *12*, 2045–2054.

[18] Papachristou, E. K., Roumeliotis, T. I., Chrysagi, A., Trigoni, C., Charvalos, E., Townsend, P. A., Pavlakis, K., Garbis, S. D., *J. Proteome Res.* 2013, *12*, 2078–2089.

[19] Wiederin, J. L., Donahoe, R. M., Anderson, J. R., Yu, F., Fox, H. S., Gendelman, H. E., Ciborowski, P. S., *J. Proteome Res.* 2010, *9*, 4721–4731.

[20] Lietzen, N., Ohman, T., Rintahaka, J., Julkunen, I., Aittokallio, T., Matikainen, S., Nyman, T. A., *PLoS Pathog.* 2011, *7*, e1001340.

[21] Zhou, J. Y., Ye, J. X., Ye, W. C., Chen, Q. X., Zheng, X. J., Guo, J. Q., *Prog. Biochem. Biophys.* 2005, *32*, 37–45.

[22] Ye, J. X., Chen, Q. X., Zhou, J. Y., Li, L. Y., *Cell Biol. Int.* 2005, *31*, 165–172.

[23] Abere, B., Wikan, N., Ubol, S., Auewarakul, P., Paemanee, A., Kittisenachai, S., Roytrakul, S., Smith, D. R., *PLoS One* 2012. *7*, e34800.

[24] Wisniewski, J. R., Zougman, A., Nagaraj, N., Mann, M., *Nat. Methods* 2009, *6*, 359–362.

[25] Munday, D. C., Emmott, E., Surtees, R., Lardeau, C. H., Wu, W., Duprex, W. P., Dove, B. K., Barr, J. N., Hiscox, J. A., *Mol. Cell. Proteomics* 2010, *9*, 2438–2459.

[26] Gan, C. S., Chong, P. K., Pham, T. K., Wright, P. C., *J. Proteome Res.* 2007, *6*, 821–827.

[27] Zhang, B. H., Liu, X. Y., Chen, W., Chen, L., *Acta Biochem. Biophys. Sin.* 2013, *45*, 867–874.

[28] Brass, A. L., Huang, I. C., Benita, Y., John, S. P., Krishnan, M. N., Feeley, E. M., Ryan, B. J., Weyer, J. L., vander Weyden, L., Fikrig, E., Adams, D. J., Xavier, R. J., Farzan, M., Elledge, S. J., *Cell* 2009, *139*, 1243–1254.

[29] Munday, D. C., Hiscox, J. A., Barr, J. N., *Proteomics* 2010, *10*, 4320–4334.

[30] Shrestha, N., Bahnan, W., Wiley, D. J., Barber, G., Fields, K. A., Schesser, K., *J. Biol. Chem.* 2012, *287*, 28738–28744.

[31] Katibah, G. E., Lee, H. J., Huizar, J. P., Vogan, J. M., Alber, T., Collins, K., *Mol. Cell.* 2013, *49*, 743–750.

[32] Karst, S. M., Wobus, C. E., Lay, M., Davidson, J., Virgin, H. W., *Science* 2003, *299*, 1575–1578.

[33] Suk, K., Kim, S., Kim, Y. H., Kim, K. A., Chang, I., Yagita, H., Shong, M., Lee, M. S., *J. Immunol.* 2001, *166*, 4481–4489.

[34] Sen, G. C., Sarkar, S. N., *Curr. Top. Microbiol.* 2007, *316*, 233–250.

[35] Zhang, L. K., Chai, F., Li, H. Y., Xiao, G., Guo, L., *J. Proteome Res.* 2013, *12*, 2666–2678.

[36] Diamond, M. S., Farzan, M., *Nat. Rev. Immunol.* 2013, *13*, 46–57.

[37] Raychoudhuri, A., Shrivastava, S., Steele, R., Kim, H., Ray, R., Ray, R. B., *J. Virol.* 2011, *85*, 12881–12889.

[38] Pichlmair, A., Lassnig, C., Eberle, C. A., Gorna, M. W., Baumann, C. L., Burkard, T. R., Burckstummer, T., Stefanovic, A., Krieger, S., Bennett, K. L., Rulicke, T., Weber, F., Colinge, J., Muller, M., Superti-Furga, G., *Nat. Immunol.* 2011, *12*, 624–632.

[39] Pinto, A. K., Daffis, S., Brien, J. D., Gainey, M. D., Yokoyama, W. M., Sheehan, K. C., Murphy, K. M., Schreiber, R. D., Diamond, M. S., *PLoS Pathog.* 2011, *7*, e1002407.

[40] Katoh, H., Mori, Y., Kambara, H., Abe, T., Fukuhara, T., Morita, E., Moriishi, K., Kamitani, W., Matsuura, Y., *J. Virol.* 2011, *85*, 10976–10988.

[41] Lee, J. W., Liao, P. C., Young, K. C., Chang, C. L., Chen, S. S. L., Chang, T. T., Lai, M. D., Wang, S. W., *J. Proteome Res.* 2011, *10*, 4522–4534.

[42] Ertel, K. J., Brunner, J. E., Semler, B. L., *J. Virol.* 2010, *84*, 4229–4242.

[43] Gustin, K. E., Sarnow, P., *Embo J.* 2001, *20*, 240–249.

[44] Gupta, A. K., Drazba, J. A., Banerjee, A. K., *J. Virol.* 1998, *72*, 8532–8540.

[45] Chevalier, C., Lepault, J., Da Costa, B., Delmas, B., *J. Virol.* 2004, *78*, 3296–3303.

[46] Edgcomb, S. P., Carmel, A. B., Naji, S., Ambrus-Aikelin, G., Reyes, J. R., Saphire, A. C. S., Gerace, L., Williamson, J. R., *J. Mol. Biol.* 2012, *415*, 61–74.

[47] Ishaq, M., Ma, L., Wu, X., Mu, Y., Pan, J., Hu, J., Hu, T., Fu, Q., Guo, D., *J. Cell Biochem.* 2009, *106*, 296–305.

[48] Xu, L., Khadijah, S., Fang, S., Wang, L., Tay, F. P., Liu, D. X., *J. Virol.* 2010, *84*, 8571–8583.

[49] Lin, C. W., Cheng, C. W., Yang, T. C., Li, S. W., Cheng, M. H., Wan, L., Lin, Y. J., Lai, C. H., Lin, W. Y., Kao, M. C., *Virus Res.* 2008, *137*, 49–55.

[50] Barber, G. N., *RNA Biol.* 2009, *6*, 35–39.

[51] Guan, D. Y., Altan-Bonnet, N., Parrott, A. M., Arrigo, C. J., Li, Q., Khaleduzzaman, M., Li, H., Lee, C. G., Pe'ery, T., Mathews, M. B., *Mol. Cell Biol.* 2008, *28*, 4629–4641.

[52] Sakamoto, S., Aoki, K., Higuchi, T., Todaka, H., Morisawa, K., Tamaki, N., Hatano, E., Fukushima, A., Taniguchi, T., Agata, Y., *Mol. Cell Biol.* 2009, *29*, 3754–3769.

[53] Yaseen, N. R., Maizel, A. L., Wang, F., Sharma, S., *J. Biol. Chem.* 1993, *268*, 14285–14293.

[54] Stricker, R. L., Behrens, S. E., Mundt, E., *J. Virol.* 2010, *84*, 10592–10605.

[55] Han, B. G., Kim, K. H., Lee, S. J., Jeong, K. C., Cho, J. W., Noh, K. H., Kim, T. W., Kim, S. J., Yoon, H. J., Suh, S. W., Lee, S., Lee, B. I., *J. Biol. Chem.* 2012, *287*, 10727–10737.

[56] Morris, E. J., Michaud, W. A., Ji, J. Y., Moon, N. S., Rocco, J. W., Dyson, N. J., *Plos Genet.* 2006, *2*, 1834–1848.

[57] Ren, K., Zhang, W., Shi, Y., Gong, J., *Pathol. Oncol. Res.* 2010, *16*, 229–237.

[58] Schwarz, K. B., *Free Radic Biol. Med.* 1996, *21*, 641–649.

[59] Tavender, T. J., Springate, J. J., Bulleid, N. J., *EMBO J.* 2010, *29*, 4185–4197.

[60] Colombo, E., Bonetti, P., Denchi, E. L., Martinelli, P., Zamponi, R., Marine, J. C., Helin, K., Falini, B., Pelicci, P. G., *Mol. Cell Biol.* 2005, *25*, 8874–8886.

[61] Grisendi, S., Bernardi, R., Rossi, M., Cheng, K., Khandker, L., Manova, K., Pandolfi, P. P., *Nature* 2005, *437*, 147–153.

[62] Samad, M. A., Okuwaki, M., Haruki, H., Nagata, K., *FEBS Lett.* 2007, *581*, 3283–3288.

[63] Ryan, K. M., Phillips, A. C., Vousden, K. H., *Curr. Opin. Cell. Biol.* 2001, *13*, 332–337.

[64] Bertwistle, D., Sugimoto, M., Sherr, C. J., *Mol. Cell Biol.* 2004, *24*, 985–996.

[65] Vizcaíno, J. A., Deutsch, E. W., Wang, R., Csordas, A., Reisinger, F., Ríos, D., Dianes, J. A., Sun, Z., Farrah, T., Bandeira, N., Binz, P. A., Xenarios, I., Eisenacher, M., Mayer, G., Gatto, L., Campos, A., Chalkley, R. J., Kraus, H. J., Albar, J. P., Martinez-Bartolomé, S., Apweiler, R., Omenn, G. S., Martens, L., Jones, A.R., Hermjakob, H., *Nat. Biotechnol.* 2014, *30*, 223–226.

